

A Structurally Coherent Spatial Phase Estimate

Brian Knight¹[0000–0001–8049–4749] and Naoki Saito¹[0000–0001–5234–4719]

Department of Mathematics, University of California, Davis, CA 95616 USA

Abstract. The monogenic signal (MS) was introduced by Felsberg and Sommer [3], and independently by Larkin [7] under the name vortex operator. It is a two-dimensional (2D) analog of the well-known analytic signal, and allows for direct amplitude and phase demodulation of (amplitude and phase) modulated images so long as the signal is intrinsically one-dimensional (i1D). Felsberg’s PhD dissertation also introduced the structure multivector (SMV), a model allowing for intrinsically 2D (i2D) structure. While the monogenic signal has become a well-known tool in the image processing community, the SMV is little used, although even in the case of i1D signals it provides a more robust orientation estimation than the MS. We argue the SMV is more suitable in standard i1D image feature extraction due to this improvement, and extend the steerable wavelet frames of Held et al. [4] to accommodate the additional features of the SMV. We then propose a novel quality map based on local orientation variance which values structurally coherent patches. This yields a multiscale phase estimate which performs well even when signal to noise ratio (SNR) is ≤ 1 . The performance is evaluated on several synthetic phase estimation tasks as well as on a fine-scale fingerprint registration task related to the 2D phase demodulation problem.

Keywords: Spatial phase · Phase Demodulation · Multiscale Methods · Monogenic Signal · Fingerprint Registration

1 Introduction

Many problems in imaging science rely on spatial phase measurements, e.g. 2D interferometry, interferometric SAR (InSAR), and require a preprocessing step to estimate the true spatial phase of an image or set of images [12]. Any improvement to this estimate will thus improve downstream analysis. A standard approach for estimating spatial phase of images is to use the phase of the *monogenic signal* [6] [13]. The first improvement to this estimate is to produce a multiscale monogenic phase estimate, see Kaseb et al. [5], for instance, which makes use of isotropic wavelets [4] [10], and provides a robust phase estimate in the presence of image corruption. **The main contributions of this article are: 1)** to employ the *structure multivector* (SMV) in place of the monogenic signal in order to extract a more robust feature set at any given scale; and **2)** to define a novel quality measure at each scale, based on the features of the SMV, in order to determine the optimal local feature set around a given point in an

image. We perform several experiments on synthetic images to showcase the application of the our multiscale phase estimation, and further solve a phase and amplitude demodulation problem in 2D to display the utility of this estimate. Additionally, we use our multiscale phase estimate in order to solve a fine-scale fingerprint registration problem as described in [1]. Lastly, we have provided a Julia module that includes the code needed to reproduce any figures and experiments shown in this paper, as well as standalone functions to perform our multiscale phase estimation: <https://gitlab.com/briancknight/SSVM2025>.

The rest of the article is organized as follows. In Section 2 we discuss the standard signal model used to describe fringe patterns, and define the monogenic signal (MS), steerable wavelets, and the structure multivector (SMV). Section 3 describes the novel multiscale phase estimate derived from the SMV features at each scale, and Section 4 concludes with numerical experiments showcasing the improved phase estimation as well as improved accuracy in 2D phase and amplitude demodulation tasks, including one used in fine-scale fingerprint registration. Section 5 provides a brief conclusion to the article. In the additional appendix, Appendix A provides more details in the construction of the structure multivector, and Appendix B provides an error analysis for the feature set of the SMV when the i2D signal model is violated.

2 Signal Models

2.1 The i1D Signal Model and the Monogenic Signal

In 1D signal processing, a real-valued signal can be extended to a complex valued signal via the Hilbert transform, and this complex-valued extension can provide useful insight into the signal’s local amplitude and frequency. In 2D, the monogenic signal is a quaternion valued signal that extends the real-valued 2D signal via the Riesz transform, the appropriate 2D extension of the Hilbert transform. If our original signal obeys the signal model

$$f(\mathbf{x}) = A(\mathbf{x}) \cos(\mathbf{n}(\mathbf{x}) \cdot \mathbf{x}), \quad \mathbf{x} \in \mathbb{R}^2 \quad (1)$$

where $A(\mathbf{x}) \geq 0$ is the local amplitude function, and $\mathbf{n}(\mathbf{x})$ is the local orientation, and $\varphi(\mathbf{x}) = \mathbf{n}(\mathbf{x}) \cdot \mathbf{x}$ is the local phase function, and we assume $A(\mathbf{x})$ varies slowly with respect to the $\cos(\mathbf{n}(\mathbf{x}) \cdot \mathbf{x})$. We may also refer to A as the *local energy*, and the tuple $(\mathbf{n}(\mathbf{x}), \varphi(\mathbf{x}))$ as the *local structure*.

The *monogenic signal* is defined as the quaternionic signal

$$f_M(\mathbf{x}) = f(\mathbf{x}) + i\mathcal{R}_1 f(\mathbf{x}) + j\mathcal{R}_2 f(\mathbf{x}),$$

where

$$\mathcal{R}_k f(\mathbf{x}) = \int_{\mathbb{R}^2} \frac{x'_k}{2\pi \|\mathbf{x}'\|^{\frac{3}{2}}} f(\mathbf{x} - \mathbf{x}') dx'_1 dx'_2,$$

is the Riesz transform for the x_k direction in \mathbb{R}^2 , and $\mathcal{R}f(\mathbf{x}) = i\mathcal{R}_1 f(\mathbf{x}) + j\mathcal{R}_2 f(\mathbf{x})$ is the (total) Riezs transform. Larkin [7] showed that for signals of the

i1D model described above, the Riesz transform obeys the asymptotic Bedrosian Principle:

$$\mathcal{R}(A(\mathbf{x}) \cos(\varphi(\mathbf{x}))) \approx A(\mathbf{x}) \mathcal{R}(\cos(\varphi(\mathbf{x}))),$$

and, further, that

$$\mathcal{R}(\cos(\varphi(\mathbf{x}))) \approx \mathbf{n}(\mathbf{x}) \sin(\varphi(\mathbf{x})),$$

In the case of $\varphi(\mathbf{x}) = 2\pi\omega\mathbf{n} \cdot \mathbf{x}$ for some unit vector \mathbf{n} and frequency ω , i.e., a plane wave, so long as $\hat{A}(\mathbf{u}) = 0$ for any \mathbf{u} such that $|\mathbf{u}| > \omega$, the Riesz transform performs the correct quadrature shift for phase estimation of i1D signals in two dimensions.

To be clear, given a signal f of the form described in (1), the monogenic signal of f is given by

$$f_M(\mathbf{x}) = A(\mathbf{x}) (\cos(\varphi(\mathbf{x})) + \mathbf{n}(\mathbf{x}) \sin(\varphi(\mathbf{x}))),$$

thus we can recover the local amplitude, local orientation, and local phase via

$$A(\mathbf{x}) = |f_M(\mathbf{x})|, \quad \mathbf{n}(\mathbf{x}) = \frac{\mathcal{R}f(\mathbf{x})}{|\mathcal{R}f(\mathbf{x})|}, \quad \varphi(\mathbf{x}) = \arctan(|\mathcal{R}f(\mathbf{x})|, f(\mathbf{x})).$$

This feature set is considered to be a *split of identity*, in that it separates a signal into independent local features. Specifically, the local structure is invariant to scaling of the local energy, and the local energy is invariant to phase shifts in the local structure. This allows for useful image processing steps, such as equalization of brightness [4], or, as we discuss later, phase modulation and demodulation.

Similarly, we can use local amplitude information in order to determine important features. This approach is particularly useful when the monogenic signal is paired with an isotropic wavelet decomposition [5], which we outline in the next section.

2.2 Steerable Wavelet Frames using Riesz Transforms

The Riesz transform \mathcal{R} is isotropic, meaning that if R_θ is a 2D rotation matrix, then $\mathcal{R}R_\theta f(\mathbf{x}) = R_\theta \mathcal{R}f(\mathbf{x})$. It also commutes with shifts and dilations so that applying any one of these operations to the signal f can be done before or after computing the monogenic extension. As far as wavelet analysis is concerned, this allows us to construct monogenic wavelets simply by constructing a real isotropic wavelet and then computing its Riesz transform.

Based on this property, Held et al. [4] construct steerable wavelet frames for n D signals which, for a given image $f \in \mathbb{R}^{2^M \times 2^M}$, yields the decomposition into $M \cdot K$ scales, where M is the number of dyadic scales, and K the number of subscales used for each dyadic scale. We denote the components of the decomposition by $d_{j,s}(\mathbf{x})$ for $j = 1, \dots, K$, $s = M', \dots, M$, where $M' \geq 1$ is the

smallest dyadic scale used (typically $M' = 3$), and an approximation component a_M which contains any remaining low-frequency information. Naturally, we can extend each scale via the Riesz transform to obtain:

$$(d_{j,s}(\mathbf{x}))_M = A_{j,s}(\mathbf{x}) [\cos(\varphi_{j,s}(\mathbf{x})) + \mathbf{n}_{j,s}(\mathbf{x}) \sin(\varphi_{j,s}(\mathbf{x}))]$$

If $K = 1$, each dyadic scale is decomposed via complementary high and low pass filters. For $K > 1$, the dyadic scale is decomposed into $K - 1$ band-pass components, and a high and low frequency component. The specific construction can be found used in [4]. Figure 1a depicts the filters for $K = 2$, while Figure 1b shows the instantaneous amplitude and phase (IAP) representation of the high frequency and band-pass component provided by the structure multivector which we discuss in the next section.

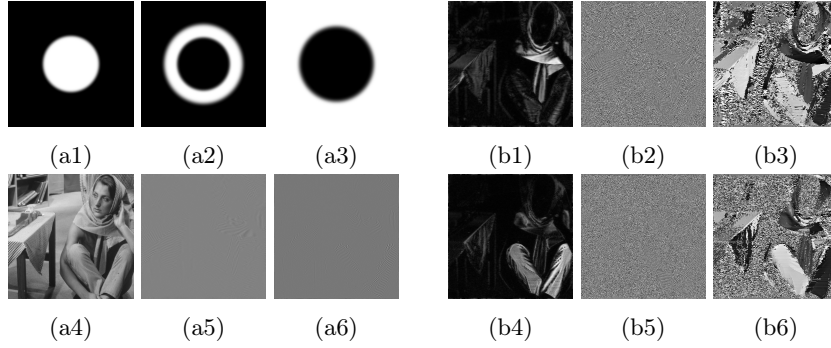


Fig. 1: Left: Isotropic wavelet frames, (a1) low-pass $h_{1,1}$, (a2) band-pass $h_{1,2}$, (a3) high-pass $h_{1,3}$. Applied to Barbara: (a4) low-pass, (a5) band-pass, (a6) high-pass. Right: IAP representation of isotropic wavelet scales, (b1) $A_{1,2}(\mathbf{x})$, (b2) $\Phi_{1,2}(\mathbf{x})$, (b3) $\theta_{1,2}(\mathbf{x})$, (b4) $A_{1,3}(\mathbf{x})$, (b5) $\Phi_{1,3}(\mathbf{x})$, (b6) $\theta_{1,3}(\mathbf{x})$

2.3 The i2D Signal Model and the Structure Multivector

Two-dimensional signals can, of course, vary in two or more orientations in any given local patch, and further work has been done using hypercomplex signal processing that can deal with these cases. One extension, the *structure multivector* (SMV), was introduced along with the monogenic signal in the PhD dissertation of Felsberg [3]. It is designed to deal with signals of the form

$$f(\mathbf{x}) = f_1(\mathbf{n}(\mathbf{x}) \cdot \mathbf{x}) + f_2(\mathbf{n}(\mathbf{x})^\perp \cdot \mathbf{x}), \quad (2)$$

These are intrinsically 2D (i2D) signals with two orientations in each local patch that are orthogonal to one another.

The features of the SMV will essentially be that of two monogenic signals, and to accommodate these additional features the SMV lives in a larger dimensional

Clifford algebra, $\mathcal{Cl}_{3,0}$ which subsumes the quaternions. This algebra is generated by the orthonormal basis e_1, e_2, e_3 satisfying the relations $e_i e_j + e_j e_i = 2\delta_{ij}$, and consists of $2^3 = 8$ elements: $1, e_1, e_2, e_3, e_{12}, e_{23}, e_{31}, e_{123}$. In general we denote the product $e_{i_1} e_{i_2} \cdots e_{i_n} := e_{i_1 i_2 \dots i_n}$. For more information on Clifford algebras and the construction of the SMV see [2], [3] and Appendix A. We only give here the minimum details needed to construct the SMV. We consider an image of the form $\mathbf{f} : \mathbb{R}^2 \rightarrow e_3 \mathbb{R}$, $\mathbf{f}(\mathbf{x}) = f(x, y)e_3$.

The corresponding structure multivector (SMV) is given by

$$\begin{aligned} M_S(\mathbf{x}) &= [\mathbf{f}(\mathbf{x}) + (h_2^1 * \mathbf{f})(\mathbf{x})] + e_3 [(h_2^2 * \mathbf{f})(\mathbf{x}) + (h_2^3 * \mathbf{f})(\mathbf{x})] \\ &= M_0 + M_1 e_1 + M_2 e_2 + M_3 e_3 + M_{23} e_{23} + M_{31} e_{31} + M_{12} e_{12}. \end{aligned} \quad (3)$$

The explicit definitions of these functions are given below, where $\mathbf{x} = x e_1 + y e_2$:

$$\begin{aligned} M_1 &= \frac{x}{2\pi|\mathbf{x}|^3} * f(\mathbf{x}), & M_2 &= \frac{y}{2\pi|\mathbf{x}|^3} * f(\mathbf{x}), & M_3 &= f(\mathbf{x}), \\ M_{23} &= \frac{3(3x^2 y - y^3)}{2\pi|\mathbf{x}|^5} * f(\mathbf{x}), & M_{31} &= \frac{3(3x y^2 - x^3)}{2\pi|\mathbf{x}|^5} * f(\mathbf{x}), \\ M_0 &= \frac{-2(x^2 - y^2)}{2\pi|\mathbf{x}|^4} * f(\mathbf{x}), & M_{12} &= \frac{-4xy}{2\pi|\mathbf{x}|^4} * f(\mathbf{x}). \end{aligned}$$

Here $h_2^1 = \mathcal{R}$ denotes the Riesz transform, h_2^3 is the composition of h_2^2 and h_2^1 , where $H_2^2(\mathbf{u}) = \frac{(u^2 - v^2) + 2uv e_{12}}{u^2}$ is the Fourier transform of h_2^2 . H_2^2 responds only to even signals, and any two perpendicular vectors \mathbf{n} and \mathbf{n}^\perp become antiparallel after action by H_2^2 , which means that an even signal according to the (2) will yield a response to H_2^2 whose argument is precisely twice that of the main orientation of \mathbf{n} .

Specifically, we can calculate the orientation \mathbf{n} given a signal of the form $f(\mathbf{x}) = A \cos(\mathbf{n} \cdot \mathbf{x}) + B \cos(\mathbf{n}^\perp \cdot \mathbf{x})$ directly from this response. To handle odd structures, we finally take the Riesz transform of h_2^2 to yield h_2^3 . The product of the Riesz response and the response of the third order harmonic estimates this same orientation, but is better suited for odd structures, hence the average of these two arguments provides a robust orientation estimate of the structure multivector, as given in Felsberg's dissertation [3]:

$$\theta_e = \frac{1}{4} \arg [(M_0 + M_{12} I_2)^2 + (M_1 + M_2 I_2)(M_{31} - M_{23} I_2)], \quad (4)$$

where $I_2 = e_{12}$ acts as the imaginary unit i .

In [3] the author shows that the extended signal model provides a more robust orientation estimate than that of the monogenic signal. This is further confirmed in [9]. In addition to these facts, we show that: 1) the feature set of the SMV is robust even to i2D signals which violate the orthogonality constraint; and 2) if one of the local i1D signal dominates the local energy, then we can estimate the corresponding orientation well even in the case of large deviation from this constraint. See Appendix B for details.

With this orientation estimate it is then possible to construct a pair of local angular filters that decompose a signal f into two i1D signals, which then yields two local amplitudes, two local orientations, and two local phases that can be used for further processing. Again, see [3] or Appendix A for full details. The output of the local angular filtering is two complex i1D signals which we denote by $F_1(\mathbf{x})$ and $F_2(\mathbf{x})$.

The full feature set of the SMV then is given by the local orientation estimate in (4) and:

$$A_i(\mathbf{x}) = |F_i(\mathbf{x})|, \quad \phi_i(\mathbf{x}) = \arg |F_i(\mathbf{x})|, \quad (5)$$

for $i = 1, 2$. At each location \mathbf{x} , we choose the main signal by selecting the pair with the largest local amplitude. This selection is given by the dominance index $d(\mathbf{x}) = \arg \max_{1,2} \{A_1(\mathbf{x}), A_2(\mathbf{x})\}$, so that we have a major and minor IAP representation given by:

$$A(\mathbf{x}) = A_{d(\mathbf{x})}(\mathbf{x}), \quad \Phi(\mathbf{x}) = \phi_{d(\mathbf{x})}(\mathbf{x}), \quad a(\mathbf{x}) = A_{3-d(\mathbf{x})}(\mathbf{x}), \quad \phi(\mathbf{x}) = \phi_{3-d(\mathbf{x})}(\mathbf{x}).$$

Here the capital A and Φ denote the dominant, or major, local i1D signal. Figure 1b depicts the major IAP representation of two scales of Barbara.

3 Multiscale Feature Estimation

3.1 A Multiscale Phase Estimate Using the Structure Multivector

Here we extend the multiscale phase extraction algorithm to use the feature set of the structure multivector. Let f be the given signal and $(f^{(k)})_{k=1}^K$ be the isotropic wavelet decomposition of f , and $A^{(k)}, \Phi^{(k)}, a^{(k)}$, and $\phi^{(k)}$ for $k = 1, \dots, K$ denote the major amplitude, major phase, minor amplitude, and minor phase of $f^{(k)}$ respectively.

If we let $\mathcal{Q}(\mathbf{x}) \geq 0$ be a *local quality function* which may depend on any aspect of the local multiscale feature set (here provided by steerable wavelets and the SMV), we can define the *local scale* to be given by

$$k^{\mathcal{Q}}(\mathbf{x}) = \arg \max_k \{\mathcal{Q}^{(k)}(\mathbf{x})\},$$

where $\mathcal{Q}^{(k)}$ is the quality function applied to the multiscale features at scale $f^{(k)}$. The corresponding local *multiscale features*

$$\begin{aligned} A_{\mathcal{Q}}(\mathbf{x}) &= A^{k^{\mathcal{Q}}(\mathbf{x})}(\mathbf{x}), & \Phi_{\mathcal{Q}}(\mathbf{x}) &= \Phi^{k^{\mathcal{Q}}(\mathbf{x})}(\mathbf{x}), & \theta_{\mathcal{Q}}(\mathbf{x}) &= \theta^{k^{\mathcal{Q}}(\mathbf{x})}(\mathbf{x}), \\ a_{\mathcal{Q}}(\mathbf{x}) &= a^{k^{\mathcal{Q}}(\mathbf{x})}(\mathbf{x}), & \phi_{\mathcal{Q}}(\mathbf{x}) &= \phi^{k^{\mathcal{Q}}(\mathbf{x})}(\mathbf{x}). \end{aligned}$$

In [5] $\mathcal{Q}^{(k)}(\mathbf{x})$ is defined to be the amplitude of the monogenic signal at that scale. The analog in this paper is the major amplitude of the SMV at each scale, which we call the *local amplitude quality*. The idea is to choose the scale with the maximum local energy; if the underlying signal in question is some sort of

well structured fringe pattern, such as an interferogram or fingerprint, this scale should correspond to the true spatial phase to be estimated and the multiscale feature set should be robust to noise or local signal corruption when the signal to noise ratio (SNR) is sufficiently well behaved.

When the local SNR is close to 1, however, the scale with the dominant amplitude is likely to be the noise itself. Still, it may be assumed that the signal corruption does not contain coherent structural information, and so we submit that a local quality metric which makes use of the local structural information should enable good phase estimation even when $\text{SNR} \leq 1$.

We propose applying local variance filter \mathcal{V} to each θ^k with an appropriate window size, where lower local variance indicates a more coherent signal. Define the *local orientation variance quality* and corresponding local scale to be:

$$\mathcal{Q}_\theta^{(k)}(\mathbf{x}) = \frac{1}{1 + \mathcal{V}_{w_k}(\theta^k)(\mathbf{x})}, \quad k\mathcal{Q}_\theta(\mathbf{x}) = \arg \max_k \{\mathcal{Q}_\theta^{(k)}(\mathbf{x})\}.$$

We set the window size w_k to be twice the dyadic scale. We also consider the *local product quality* given by the product of the local amplitude quality and local orientation variance quality, $\mathcal{Q}_\theta^{(k)}(\mathbf{x}) \cdot A^{(k)}(\mathbf{x})$, as this utilizes both local energy and local structure information. Figure 2 compares the results of these three quality functions for the spatial phase estimate of a real fingerprint. We further compare phase estimation results of a plane wave signal and a parabolic chirp signal, which are shown alongside their respective spatial phases in Figure 3. The details of our experiments are outlined further in Section 4.

4 Experiments

This section provides results of the proposed multiscale phase estimation algorithm applied to several standard phase estimation problems: 1) a baseline experiment on estimating the phase of plane waves of different frequencies; 2) estimating the phase of a parabolic chirp, a standard signal with varying local frequency, which provides a more challenging multiscale phase estimation problem; 3) 2D phase demodulation; and 4) a practical example of phase demodulation as it applies to fine-scale fingerprint registration for the problem of fingerprint matching.

4.1 Multiscale Phase Estimation Experiments

Given a noisy plane wave of the form $f(\mathbf{x}) = \cos(\omega(\mathbf{n} \cdot \mathbf{x})) + \eta_\sigma(\mathbf{x})$, where $\eta_\sigma(\mathbf{x})$ is a Gaussian random variable with mean zero and standard deviation σ , the goal is to estimate the true phase function $\omega(\mathbf{n} \cdot \mathbf{x}) \bmod 2\pi$. In our experiment we discretize so that $\mathbf{x}[i, j] = [-\pi + \frac{2\pi i}{N}, -\pi + \frac{2\pi j}{N}]$, for $i, j = 0, N-1$, for $N = 2^M$, ω ranges between 2^3 and 2^{M-2} , and $\mathbf{n} = [\cos(\pi/4), \sin(\pi/4)]^T$. We use the *structural simlary index measure* (SSIM) [11] to compare the quality of the estimated phase to the ground truth. Figure 4 shows the quality of the estimated phase for $0 \leq \sigma \leq 1.5$. Because the true amplitude of the noiseless

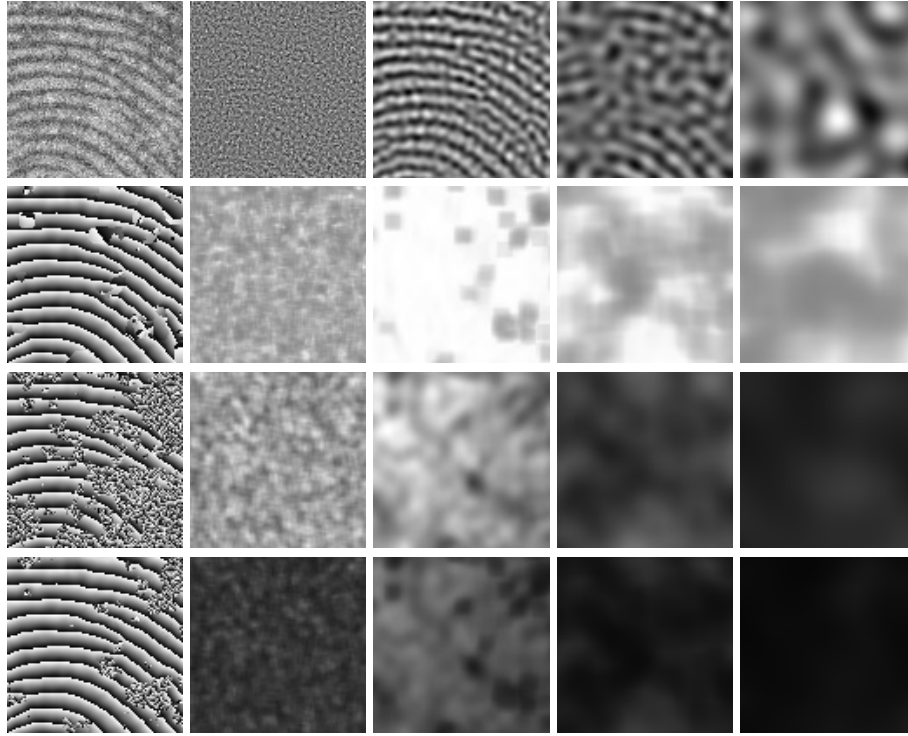


Fig. 2: Top row: noisy fingerprint and decomposition into 4 scales. Second row: multiscale phase computed via $\mathcal{Q}_\theta^{(k)}(\mathbf{x})$, local orientation variance quality of each scale. Third row: the multiscale phase computed via $A^{(k)}(\mathbf{x})$, local amplitude of each scale. Fourth row: the multiscale phase of the product $\mathcal{Q}_\theta^{(k)}(\mathbf{x}) \cdot A^{(k)}(\mathbf{x})$, product quality at each scale

signal is 1 everywhere, σ can be thought of as the reciprocal of SNR, hence $\sigma = 1$ is the point at which the Gaussian noise begins to dominate the underlying plane wave structure. The amplitude-based multiscale phase of the monogenic signal and SMV perform well until σ surpasses 0.75, beyond which the estimate is unusable. In contrast, the estimate from the local orientation variance quality and the estimate given by the product of the amplitude and local orientation variance quality provide high-quality phase estimates well beyond this point. Additionally, we test our phase estimation procedure on a *parabolic chirp*. The appeal of this signal is that the spatial frequency varies locally, and so it is a more challenging phase estimation task. Estimating the phase of such a signal is actually a known strength of the monogenic signal [5]. We demonstrate again that in the presence of signal corruption the monogenic signal fails quickly, but our multiscale approach finds the coherent local structure reliably. Furthermore, because the monogenic signal (SMV) handles locally varying frequency well, we

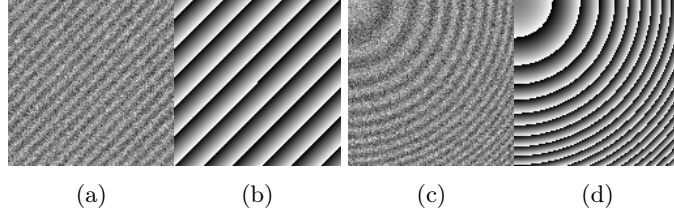


Fig. 3: Example of (a) noisy plane wave and (b) the true underlying phase, and (c) a parabolic chirp signal along with (d) its true phase

posit using an “overcomplete” set of features can improve phase estimation. We use a set of features which includes the low-pass component at each dyadic scale.

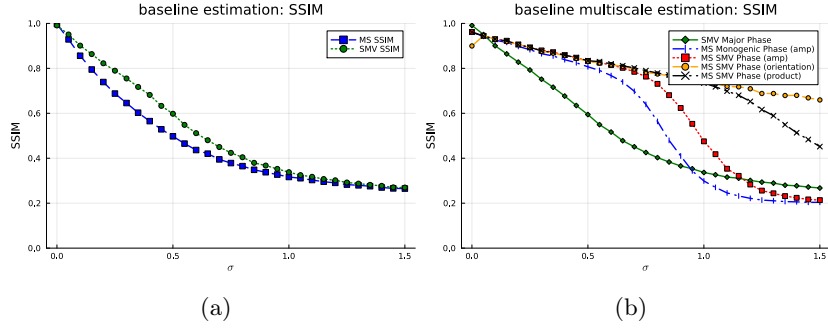


Fig. 4: phase estimation of noisy plane wave (a) comparison of MS phase vs. SMV phase (b) comparison of four multiscale phase estimates

Figure 5 shows the results of the multiscale estimate and the overcomplete multiscale estimate for varying SNR.

4.2 Phase Demodulation with Multiscale Major Phase

The multiscale major phase estimate given by the the multiscale SMV representation of a signal f motivates further experiments in phase demodulation. In two dimensions, the phase demodulation problem can be stated as follows: Given the carrier wave $c(\mathbf{x}) = A \cos(\omega_c \mathbf{n} \cdot \mathbf{x} + \phi_c)$, and a message $m(\mathbf{x})$ where $\hat{m}(\mathbf{u}) = 0$ for $|\mathbf{u}| \geq \omega_c$, the phase modulated (PM) signal is given by:

$$c_{PM}(\mathbf{x}) = \cos(\omega_c \mathbf{n} \cdot \mathbf{x} + \phi_c + m(\mathbf{x})). \quad (6)$$

Typically the message is also sinusoidal in structure. For a baseline phase demodulation task, we attempt to recover a sinusoidal message after phase modulation and noise corruption. In this case, motivated by the phase estimation

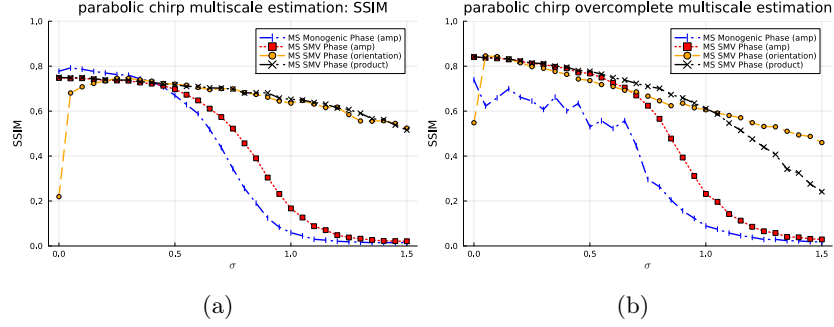


Fig. 5: Phase estimation of noisy parabolic chirp (a) comparison of four multiscale phase estimates (b) comparison of same multiscale estimation procedures with an overcomplete set of scales

of the parabolic chirp, we use the overcomplete feature set when computing the multiscale phase to more accurately capture the overlapping frequency bands resulting from the phase modulation. After estimating the modulated phase, $\tilde{\Phi}$, it is unwrapped to produce $\tilde{\Phi}^u$. If successful, the message should be well estimated by either $\pm\tilde{\Phi}^u - \omega_c \mathbf{n} \cdot \mathbf{x}$. The \pm here is due to sign ambiguity in the phase demodulation problem; for synthetic experiments the ground truth message allows us to choose the proper sign. Figure 6 shows the noisy phase modulated message, the ground truth message, and recovered messages via an amplitude based multiscale phase estimate versus the proposed product method. Again our tests conclude the product quality map allows for accurate phase estimation even when SNR is large.

4.3 Application to Deformable Fingerprint Registration

In 2018 Cui et al [1] proposed a method for fine-scale fingerprint registration via phase demodulation. The method is as follows, given a fixed and moving image, f_f and f_m , which have already been coarsely registered, we consider f_f to be the carrier wave and f_m to be a phase-modulated signal, where the message represents the unknown displacement vector field. Let $T(\mathbf{x})$ represent this displacement vector field between $f_f(\mathbf{x})$ and $f_m(\mathbf{x})$ such that $f_f(\mathbf{x} + T(\mathbf{x})) = f_m(\mathbf{x})$. Let $\mathbf{x}' = \mathbf{x} + T(\mathbf{x})$. Compute ϕ_f and ϕ_m , the (wrapped) spatial phase of the fixed and moving image respectively, and let $\Delta\phi = \phi_f - \phi_m$. Then $\Delta\phi^u$, the unwrapped phase differences, combined with local frequency information can be used to compute a spatial displacement at each coordinate, which enable the fine-scale deformable registration step. More explicitly, we let $f_f(\mathbf{x}) = \cos(\phi_f^u(\mathbf{x}))$ and $f_m(\mathbf{x}) = \cos(\phi_m^u(\mathbf{x}))$ and assume that near $\mathbf{x} = \mathbf{x}_0$ we have the estimate $\phi(\mathbf{x}) = 2\pi\omega \mathbf{n} \cdot \mathbf{x}$. Then $f_m(\mathbf{x}) = f_f(\mathbf{x}') = \cos(2\pi\omega \mathbf{n} \cdot \mathbf{x} + 2\pi\omega \mathbf{n} \cdot T(\mathbf{x}))$ and $\Delta\phi^u(\mathbf{x}) = 2\pi\omega \mathbf{n} \cdot T(\mathbf{x})$, so we recover $\mathbf{n} \cdot T(\mathbf{x}) = \frac{\Delta\phi^u(\mathbf{x})}{2\pi\omega}$, which gives the magnitude of the projection of $T(\mathbf{x})$ along the local orientation $\mathbf{n} = [\cos(\theta) \sin(\theta)]^T$. If we restrict

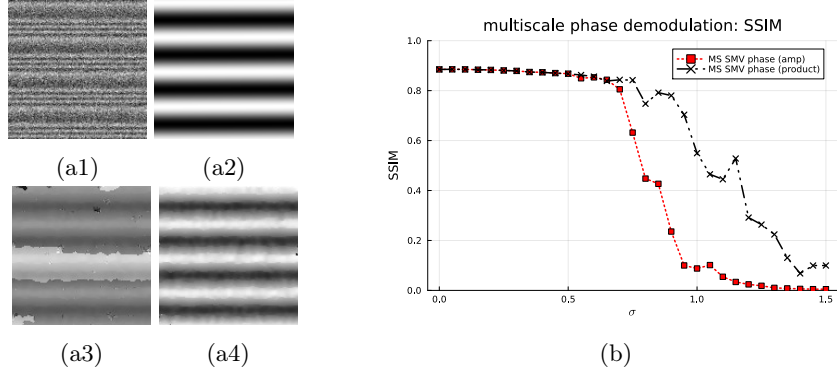


Fig. 6: Phase demodulation results: (a1) noisy phase modulated message, $\sigma = 0.75$, (a2) ground truth message, (a3) recovered via MS SMV amplitude quality, (a4) recovered via MS SMV product quality (b) comparison of MS SMV phase estimate using the amplitude quality (square markers) versus product quality (x markers)

our displacement along this direction, then, we have

$$d_x(\mathbf{x}) = \frac{\Delta\phi^u(\mathbf{x})}{2\pi\omega} \cos(\theta), \quad d_y(\mathbf{x}) = \frac{\Delta\phi^u(\mathbf{x})}{2\pi\omega} \sin(\theta). \quad (7)$$

When we have estimates of the local phase, orientation, and frequency, this becomes

$$d_x(\mathbf{x}) = \frac{\Delta\phi^u(\mathbf{x})}{2\pi\omega(\mathbf{x})} \cos(\theta(\mathbf{x})), \quad d_y(\mathbf{x}) = \frac{\Delta\phi^u(\mathbf{x})}{2\pi\omega(\mathbf{x})} \sin(\theta(\mathbf{x})). \quad (8)$$

Global phase unwrapping algorithms typically have several major discontinuities which provide unreliable frequency information. In our experiments we compute a local frequency estimate $\omega(\mathbf{x})$ by differentiation of a windowed phase unwrapping of $\Delta\phi(\mathbf{x})$. The phase and orientation values used are those provided by our multiscale method. Figure 7 gives an example of the fine-scale registration produced by this method (all images from FVC2004 DB1-B [8]).

Table 1: Correlation Values before and after fine-scale registration for various noise levels.

Type	Affine	Fine-scale	Difference
$\sigma = 0.0$	0.76	0.83	0.070
$\sigma = 0.1$	0.72	0.80	0.076
$\sigma = 0.2$	0.62	0.71	0.086
$\sigma = 0.3$	0.51	0.60	0.091
$\sigma = 0.4$	0.41	0.50	0.085
$\sigma = 0.5$	0.33	0.40	0.070

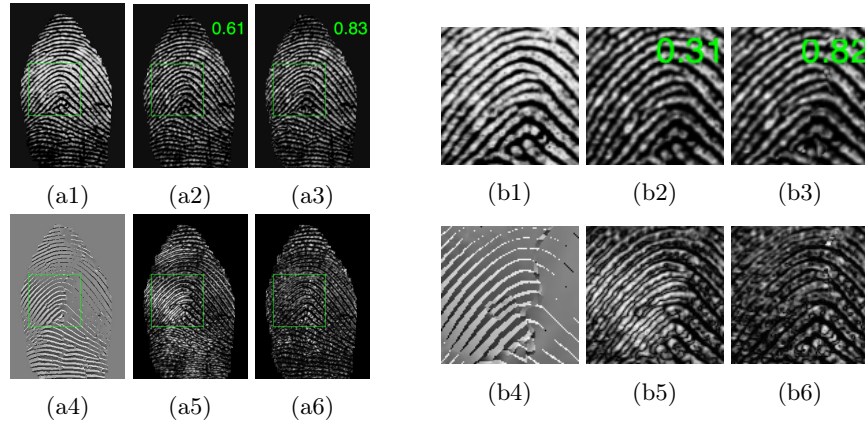


Fig. 7: (a1) fixed image, (a2) moving image, (a3) registered image, (a4) difference of multiscale phases, (a5) $|f_m(\mathbf{x}) - f_f(\mathbf{x})|$ (a6) $|f_r(\mathbf{x}) - f_f(\mathbf{x})|$. (b1) fixed image, (b2) moving image (b3) registered image, (b4) difference of multiscale phases, (b5) $|f_m(\mathbf{x}) - f_f(\mathbf{x})|$ (b6) $|f_r(\mathbf{x}) - f_f(\mathbf{x})|$. The overlaid numbers indicate the correlation coefficient with respect to the fixed image.

Table 1 expresses the quality of the fingerprint match after successful rigid registration of fingerprints, and then after the additional fine-scale deformable registration is applied. Because we are interested only in the performance of the fine-scale registration algorithm, we add noise only after successful rigid registration. We find that even at large noise levels we are able to estimate accurate fine-scale registration in well structured areas of the fingerprints.

5 Conclusion

We have argued that the Structure Multivector is a robust method for estimating the local energy and structure of fringe and interference patterns, and further define a local quality metric which rewards areas of coherent local structure. The result is a robust spatial phase estimation algorithm which allows for accurate spatial phase estimation even as noise begins to dominate the signal. We have demonstrated this with several synthetic examples and in a practical setting of fine-scale fingerprint registration.

Acknowledgments. This research was partially supported by the US National Science Foundation grants DMS-1912747 and CCF-1934568 as well as the US Office of Naval Research grant N00014-20-1-2381.

Disclosure of Interests. The authors have no competing interests to declare that are relevant to the content of this article.

References

1. Cui, Z., Feng, J., Li, S., Lu, J., Zhou, J.: 2-d phase demodulation for deformable fingerprint registration. *IEEE Transactions on Information Forensics and Security* **13**(12), 3153–3165 (2018). <https://doi.org/10.1109/TIFS.2018.2841849>
2. Delanghe, R.: Clifford Analysis: History and Perspective. *Computational Methods and Function Theory* **1**(1), 107–153 (Sep 2001). <https://doi.org/10.1007/BF03320981>
3. Felsberg, M.: Low-Level Image Processing with the Structure Multivector. Ph.D. thesis, University of Kiel, Kiel (2002)
4. Held, S.e.a.: Steerable wavelet frames based on the Riesz transform. *Journal of the Optical Society of America A* **19**(3) (Mar 2010). <https://doi.org/10.1109/TIP.2009.2036713>
5. Kaseb, M., Mercère, G., Biermé, H., Brémand, F., Carré, P.: Phase estimation of a 2D fringe pattern using a monogenic-based multiscale analysis. *Journal of the Optical Society of America A* **36**(11), C143 (Nov 2019). <https://doi.org/10.1364/JOSAA.36.00C143>
6. Kulkarni, R., Rastogi, P.: Two-step phase shifting interferometry based on orientation selective monogenic filtering. *Optics Communications* **450**, 208–215 (2019). <https://doi.org/https://doi.org/10.1016/j.optcom.2019.05.069>
7. Larkin, K.e.a.: Natural demodulation of two-dimensional fringe patterns. i. general background of the spiral phase quadrature transform. *Journal of the Optical Society of America A* **18**(8) (Aug 2001). <https://doi.org/10.1364/JOSAA.36.00C143>
8. Maio, D., Maltoni, D., Cappelli, R., Wayman, J.L., Jain, A.K.: Fvc2004: Third fingerprint verification competition. In: Zhang, D., Jain, A.K. (eds.) *Biometric Authentication*. pp. 1–7. Springer Berlin Heidelberg, Berlin, Heidelberg (2004)
9. Marchant, R., Jackway, P.: A sinusoidal image model derived from the circular harmonic vector. *Journal of Mathematical Imaging and Vision* **57** (02 2017). <https://doi.org/10.1007/s10851-016-0671-7>
10. Unser, M., Chenouard, N.: A unifying parametric framework for 2d steerable wavelet transforms. *SIAM Journal on Imaging Sciences* **6**(1), 102–135 (2013). <https://doi.org/10.1137/120866014>
11. Wang, Z., Bovik, A., Sheikh, H., Simoncelli, E.: Image quality assessment: from error visibility to structural similarity. *IEEE Transactions on Image Processing* **13**(4), 600–612 (2004). <https://doi.org/10.1109/TIP.2003.819861>
12. Zhao, C., Dong, Y., Wu, W., Tian, B., Zhou, J., Zhang, P., Gao, S., Yu, Y., Huang, L.: A modification to phase estimation for distributed scatterers in InSAR data stacks. *Remote Sensing* **15**(3) (2023). <https://doi.org/10.3390/rs15030613>
13. Zhao, L., Li, Q., Li, B.: SAR target recognition via monogenic signal and Gaussian process model. *Mathematical Problems in Engineering* **2022**(1), 3086486 (2022). <https://doi.org/https://doi.org/10.1155/2022/3086486>

A Construction of the SMV

Two-dimensional signals can, of course, vary in two or more orientations in any given local patch, and further work has been done using hypercomplex signal processing that can deal with these cases. One extension, the *structure multivector* (SMV), was introduced along with the monogenic signal in the PhD dissertation of Felsberg [3]. It is designed to deal with signals of the form

$$f(\mathbf{x}) = f_1(\mathbf{n}(\mathbf{x}) \cdot \mathbf{x}) + f_2(\mathbf{n}(\mathbf{x})^\perp \cdot \mathbf{x}), \quad (9)$$

These are intrinsically 2D (i2D) signals with two orientations in each local patch that are orthogonal to one another.

The features of the SMV will essentially be that of two monogenic signals, and to accommodate these additional features the SMV lives in a larger dimensional Clifford algebra, $\text{Cl}_{3,0}$ which subsumes the quaternions. For more information on Clifford algebras see [2], [3]. In general we denote the product $e_{i_1} e_{i_2} \cdots e_{i_n} := e_{i_1 i_2 \cdots i_n}$.

We consider an image of the form $\mathbf{f} : \mathbb{R}^2 \rightarrow e_3 \mathbb{R}$,

$$\mathbf{f}(xe_1 + ye_2) = f(x, y)e_3.$$

Note $f = \mathbf{f}e_3 = e_3\mathbf{f}$.

The corresponding structure multivector (SMV) is given by

$$\begin{aligned} M_S(\mathbf{x}) &= [\mathbf{f}(\mathbf{x}) + (h_2^1 * \mathbf{f})(\mathbf{x})] + e_3 [(h_2^2 * \mathbf{f})(\mathbf{x}) + (h_2^3 * \mathbf{f})(\mathbf{x})] \\ &= M_0 + M_1 e_1 + M_2 e_2 + M_3 e_3 + M_{23} e_{23} + M_{31} e_{31} + M_{12} e_{12} \end{aligned}$$

The explicit definitions of these functions are given below, where $\mathbf{x} = xe_1 + ye_2$:

$$\begin{aligned} M_1 &= \frac{x}{2\pi|\mathbf{x}|^3} * f(\mathbf{x}), & M_2 &= \frac{y}{2\pi|\mathbf{x}|^3} * f(\mathbf{x}), & M_3 &= f(\mathbf{x}), \\ M_{23} &= \frac{3(3x^2y - y^3)}{2\pi|\mathbf{x}|^5} * f(\mathbf{x}), & M_{31} &= \frac{3(3xy^2 - x^3)}{2\pi|\mathbf{x}|^5} * f(\mathbf{x}), \\ M_0 &= \frac{-2(x^2 - y^2)}{2\pi|\mathbf{x}|^4} * f(\mathbf{x}), & M_{12} &= \frac{-4xy}{2\pi|\mathbf{x}|^4} * f(\mathbf{x}). \end{aligned}$$

The Fourier transforms of the operators h_2^k are given below:

$$\begin{aligned} H_2^1(\mathbf{u}) &= \frac{\mathbf{u}}{|\mathbf{u}|} I_2^{-1} = \frac{-ue_2 + ve_1}{|\mathbf{u}|} \\ H_2^2(\mathbf{u}) &= \frac{e_1 \mathbf{u} e_1 \mathbf{u}}{\mathbf{u}^2} = \frac{(u^2 - v^2) + 2uve_{12}}{\mathbf{u}^2} \\ H_2^3(\mathbf{u}) &= \frac{ue_1 \mathbf{u} e_1 \mathbf{u}}{|\mathbf{u}|^3} I_2^{-1} = \frac{(3uv^2 - u^3)e_{23} - (3u^2v - v^3)e_{31}}{|\mathbf{u}|^3}, \end{aligned}$$

where $I_2 = e_{12}$ and $I_2^{-1} = e_{21}$ as $e_{12}e_{21} = 1$ by definition. I_2 acts an imaginary unit here, as $I_2^2 = -1$. Note h_2^1 is simply the Riesz transform, and h_2^3 is the composition of h_2^2 and the Riesz transform, so the crux of this extension is in understanding H_2^2 . First, it responds only to even signals. Second, any two perpendicular vectors \mathbf{n} and \mathbf{n}^\perp are antiparallel after action by H_2^2 , which means that an even signal according to the (9) will yield a response to H_2^2 whose argument is precisely twice that of the main orientation of \mathbf{n} .

Specifically, we can calculate the orientation \mathbf{n} given a signal of the form $f(\mathbf{x}) = A \cos(\mathbf{n} \cdot \mathbf{x}) + B \cos(\mathbf{n}^\perp \cdot \mathbf{x})$ directly from this response. To handle odd structures, we finally take the Riesz transform of h_2^2 to yield h_2^3 . The product of the Riesz response and the response of the third order harmonic estimates this same orientation, but is better suited for odd structures, hence the average of these two arguments provides a robust orientation estimate of the structure multivector, as given in Felsberg's dissertation [3]:

$$\theta_e = \frac{1}{4} \arg [(M_0 + M_{12}I_2)^2 + (M_1 + M_2I_2)(M_{31} - M_{23}I_2)]. \quad (10)$$

In [3] he shows that the extended signal model provides a more robust orientation estimator than that of the monogenic signal. This is further confirmed in [9]. In addition to these facts, we show that: 1) the feature set of the SMV is robust even to i2D signals which violate the orthogonality constraint; and 2) if one of the local i1D signal dominates the local energy, then we can estimate the corresponding orientation well even in the case of large deviation from this constraint. See Appendix B for details.

With this orientation estimate it is then possible to construct a pair of angular filters that decompose a signal f into two i1D signals, which will then yield two local amplitudes, two local orientations, and two local phases that can be used for further processing.

Explicitly, these filters are given by:

$$\begin{aligned} \mathcal{W}_1 f &= \frac{M_3 + \cos(2\theta_e)M_0 + \sin(2\theta_e)M_{12}}{2} \\ \mathcal{W}_2 f &= \frac{M_3 - \cos(2\theta_e)M_0 - \sin(2\theta_e)M_{12}}{2} \end{aligned}$$

and their Riesz transforms, projected onto $-e_2$:

$$\begin{aligned} \mathcal{W}_3 f &= \frac{3(\cos(\theta_e)M_1 + \sin(\theta_e)M_2) + \cos(3\theta_e)M_{31} - \sin(3\theta_e)M_{23}}{4} I_2 \\ \mathcal{W}_4 f &= \frac{3(-\sin(\theta_e)M_1 + \cos(\theta_e)M_2) + \sin(3\theta_e)M_{31} + \cos(3\theta_e)M_{23}}{4} I_2. \end{aligned}$$

Then our two complex i1D signals are given by

$$F_1(\mathbf{x}) = \mathcal{W}_1 f + \mathcal{W}_3 f, \quad F_2(\mathbf{x}) = \mathcal{W}_2 f + \mathcal{W}_4 f$$

Recall our orientation θ_e is a function of the spatial variable \mathbf{x} and is implicit in the above signals; see Eq. (4) (or Eq. (10)).

The full feature set of the SMV then is given by this local orientation estimate and:

$$A_i(\mathbf{x}) = |F_i(\mathbf{x})|, \quad \phi_i(\mathbf{x}) = \arg |F_i(\mathbf{x})|,$$

for $i = 1, 2$. At each location \mathbf{x} , we choose the main signal by selecting the pair with the largest local amplitude. This selection is given by the dominance index $d(\mathbf{x}) = \arg \max_{1,2} \{A_1(\mathbf{x}), A_2(\mathbf{x})\}$, so that we have a major and minor IAP representation given by:

$$\begin{aligned} A(\mathbf{x}) &= A_{d(\mathbf{x})}, & \Phi(\mathbf{x}) &= \phi_{d(\mathbf{x})}, \\ a(\mathbf{x}) &= A_{3-d(\mathbf{x})}, & \phi(\mathbf{x}) &= \phi_{3-d(\mathbf{x})}. \end{aligned}$$

Here the capital A and Φ denote the dominant, or major, local 1D signal.

B Orientation Estimation with the SMV

Our signal model (2) (also (9)) assumes the sum of two orthogonal sinusoidal modes, and we would like to know how this orientation estimate behaves if they are not perfectly orthogonal. We will restrict ourselves to the case where they have equal frequency so that they are inseparable even in the multiscale phase model.

Suppose $\mathbf{n} = \cos(\theta)e_1 + \sin(\theta)e_2$, $\mathbf{n}_\epsilon^\perp = \sin(\theta + \epsilon)e_1 - \cos(\theta + \epsilon)e_2$, and

$$f(\mathbf{x}) = A \cos(\mathbf{n} \cdot \mathbf{x}) + B \cos(\mathbf{n}_\epsilon^\perp \cdot \mathbf{x}).$$

We have the following:

$$\begin{aligned} M_1 + M_2 I_2 &= A(e_1 \mathbf{n}) \sin(\mathbf{n} \cdot \mathbf{x}) + B e_1 \mathbf{n}_\epsilon^\perp \sin(\mathbf{n}_\epsilon^\perp \cdot \mathbf{x}) \\ M_0 + M_{12} I_2 &= A(e_1 \mathbf{n})^2 \cos(\mathbf{n} \cdot \mathbf{x}) + B(e_1 \mathbf{n}_\epsilon^\perp)^2 \cos(\mathbf{n}_\epsilon^\perp \cdot \mathbf{x}) \\ M_{31} - M_{23} I_2 &= A(e_1 \mathbf{n})^3 \sin(\mathbf{n} \cdot \mathbf{x}) + B(e_1 \mathbf{n}_\epsilon^\perp)^3 \sin(\mathbf{n}_\epsilon^\perp \cdot \mathbf{x}), \end{aligned}$$

where

$$\begin{aligned} e_1 \mathbf{n}_\epsilon^\perp &= -I_2 \exp(\theta I_2) \exp(\epsilon I_2) \\ &= -I_2 \exp(\epsilon I_2) (e_1 \mathbf{n}) \\ (e_1 \mathbf{n}_\epsilon^\perp)^2 &= -\exp(2\theta I_2) \exp(2\epsilon I_2) \\ &= -\exp(2\epsilon I_2) (e_1 \mathbf{n})^2 \\ (e_1 \mathbf{n}_\epsilon^\perp)^3 &= I_2 \exp(3\theta I_2) \exp(3\epsilon I_2) \\ &= I_2 \exp(3\epsilon I_2) (e_1 \mathbf{n})^3. \end{aligned}$$

Analyzing the even response first, we have

$$\begin{aligned} (M_0 + M_{12} I_2)^2 &= (e_1 \mathbf{n})^4 \\ &= [A^2 \cos^2(\mathbf{n} \cdot \mathbf{x}) + B^2 \exp(4\epsilon I_2) \cos^2(\mathbf{n}_\epsilon^\perp \cdot \mathbf{x}) \\ &\quad + 2AB \exp(2\epsilon I_2) \cos(\mathbf{n} \cdot \mathbf{x}) \cos(\mathbf{n}_\epsilon^\perp \cdot \mathbf{x})]. \end{aligned}$$

For the product of odd responses we have:

$$\begin{aligned} (M_1 + M_2 I_2)(M_{31} - M_{23} I_2) &= (e_1 \mathbf{n})^4 [A^2 \sin^2(\mathbf{n} \cdot \mathbf{x}) \\ &\quad + B^2 \exp(4\epsilon I_2) \sin^2(\mathbf{n}_\epsilon^\perp \cdot \mathbf{x}) + AB(\exp(3\epsilon I_2) \\ &\quad + \exp(\epsilon I_2)) \sin(\mathbf{n} \cdot \mathbf{x}) \sin(\mathbf{n}_\epsilon^\perp \cdot \mathbf{x})]. \end{aligned}$$

In general for any real number a we have: $\exp(ai) + \exp(3ai) = 2 \exp(2ai) \cos(a)$, our odd response becomes

$$\begin{aligned} (M_1 + M_2 I_2)(M_{31} - M_{23} I_2) &= (e_1 \mathbf{n})^4 [A^2 + B^2 \exp(4\epsilon I_2) \\ &\quad + 2AB \exp(2\epsilon I_2) [\cos(\mathbf{n} \cdot \mathbf{x}) \cos(\mathbf{n}_\epsilon^\perp \cdot \mathbf{x}) + \\ &\quad \cos(\epsilon) \sin(\mathbf{n} \cdot \mathbf{x}) \sin(\mathbf{n}_\epsilon^\perp \cdot \mathbf{x})]]. \end{aligned}$$

Therefore, letting $M = \cos(\mathbf{n} \cdot \mathbf{x}) \cos(\mathbf{n}_\epsilon^\perp \cdot \mathbf{x}) + \cos(\epsilon) \sin(\mathbf{n} \cdot \mathbf{x}) \sin(\mathbf{n}_\epsilon^\perp \cdot \mathbf{x})$ for brevity, our estimate is give by:

$$\begin{aligned} \Theta(\epsilon) &= \theta + \frac{1}{4} \arg[A^2 + B^2 \exp(4\epsilon I_2) + 2AB \exp(2\epsilon I_2) \cdot M] \\ &= \theta + \frac{1}{4} \tan^{-1} \left[\frac{B^2 \sin(4\epsilon) + 2AB \sin(2\epsilon) \cdot M}{A^2 + B^2 \cos(4\epsilon) + 2AB \cos(2\epsilon) \cdot M} \right]. \end{aligned}$$

We see that as $\frac{B}{A} \rightarrow 0$ it follows that $\Theta(\epsilon) \rightarrow \theta$.

Additionally, in the case $A = B$, the argument in the artan function becomes

$$\begin{aligned} \frac{\sin(4\epsilon) + 2 \sin(2\epsilon) \cdot M}{1 + \cos(4\epsilon) + 2 \cos(2\epsilon) \cdot M} &= \frac{2 \sin(2\epsilon) [\cos(2\epsilon) + M]}{2 \cos(2\epsilon) [\cos(2\epsilon) + M]} \\ &= \tan(2\epsilon). \end{aligned}$$

Thus

$$\Theta(\epsilon) = \theta + \frac{\epsilon}{2}.$$

for $|\epsilon| < \pi/4$.